J|A|C|S
ARTICLES
Published on Web 06/15/2004

Nonspecific Medium Effects versus Specific Group Positioning in the Antibody and Albumin Catalysis of the Base-Promoted Ring-Opening Reactions of Benzisoxazoles

Yunfeng Hu,[†] K. N. Houk,*[,†] Kazuya Kikuchi,[‡] Kinya Hotta,[‡] and Donald Hilvert*[,‡]

Contribution from the Department of Chemistry and Biochemistry, University of California, Los Angeles, Los Angeles, California 90095-1569 and Department of Chemistry, Scripps Research Institute, La Jolla, California 92037, and Laboratorium für Organische Chemie, Swiss Federal Institute of Technology, ETH−Hönggerberg, CH-8093, Zürich, Switzerland

Received February 18, 2004; E-mail: houk@chem.ucla.edu; hilvert@org.chem.ethz.ch

Abstract: The mechanisms by which solvents, antibodies, and albumins influence the rates of base-catalyzed reactions of benzisoxazoles have been explored theoretically. New experimental data on substituent effects and rates of reactions in several solvents, in an antibody, and in an albumin are reported. Quantum mechanical calculations were carried out for the reactions in water and acetonitrile, and docking of the transition state into a homology model of antibody 34E4 and an X-ray structure of human serum albumin was accomplished. A microenvironment made up of catalytic polar groups (glutamate in antibody 34E4 and lysine in human serum albumin) surrounded by relatively nonpolar groups is present in both catalytic proteins.

Introduction

The conversions of benzisoxazoles to cyanophenoxides with bases and various catalysts, often referred as the "Kemp elimination,"[1a−b] have been used as a probe of medium effects on the rates of reactions (Figure 1). The rates of these reactions are very sensitive to solvent polarity. Kemp and co-workers' classic studies of the effect of substituents and solvents established that the acetate-promoted reaction of 5-nitrobenzisoxazole is 10^8 times faster in acetonitrile than water.[1c−d] This reaction has subsequently been shown to be catalyzed by catalytic antibodies ($k_{cat}/k_{uncat} = 10^6$),[2] serum albumins (10^3),[3−5] orphan antibodies (10^3),[6] a polyamine organic host (10^3),[7] surfactant vesicles (850),[8] micelles (400),[8] polyethyleneimine "synzymes" (10^5 per site),[9] and even coal (200).[10] Because different authors use different definitions for k_{cat} and k_{uncat}, those accelerations are not always directly comparable. For example, k_{uncat} can be considered as a pseudo-first-order rate constant of a water catalyzed reaction, or a second-order rate constant of an acetate or amine base-promoted reaction in water, whereas k_{cat} can be either a second-order rate constant in base-promoted reactions in different solvents or a first-order rate constant when saturated protein catalysts are involved. The various rate constants in different catalytic systems and the k_{uncat} used to compute them are listed in Table 1. The magnitude of the rate acceleration clearly depends on the pK_a of the base responsible for deprotonation and hence on the pH of the reaction medium. Catalysts such as antibody 34E4 and the polyethyleneimine "synzymes" exhibit high rate accelerations at pH values near their pK_a (ca. 6), whereas catalysts such as BSA with higher pK_a's (ca. 10) must contend with the high background rate at

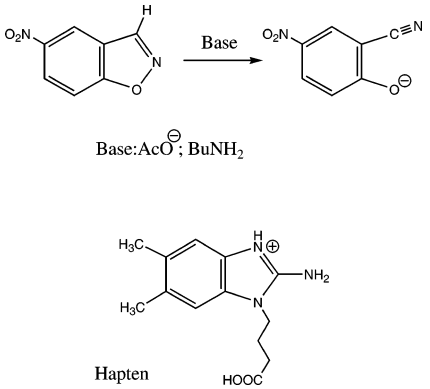

Figure 1. Base-catalyzed decomposition of benzisoxazoles (the "Kemp elimination") and the hapten used to elicit antibody 34E4.

[†] University of California, Los Angeles.
[‡] Scripps Rsearch Institute and Swiss Federal Institute of Technology.

(1) (a) Casey, M. L.; Kemp, D. S.; Paul, K. G.; Cox, D. D. *J. Org. Chem.* **1973**, *38*, 2294−2301. (b) Kemp, D. S.; Casey, M. L. *J. Am. Chem. Soc.* **1973**, *95*, 6670−6680. (c) Kemp, D. S.; Paul, K. *J. Am. Chem. Soc.* **1975**, *97*, 7305−7312. (d) Kemp, D. S.; Cox, D. D.; Paul, K. *J. Am. Chem. Soc.* **1975**, *97*, 7312−7318.
(2) Thorn, S. N.; Daniels, R. G.; Auditor, M.-T. M.; Hilvert, D. *Nature* **1995**, *373*, 228−230.
(3) Hollfelder, F.; Kirby, A. J.; Tawfik, D. S. *Nature* **1996**, *383*, 60−63.
(4) Kikuchi, K.; Thorn, S. N.; Hilvert, D *J. Am. Chem. Soc.* **1996**, *118*, 8184−8185.
(5) Hollfelder, F.; Kirby, A. J.; Tawfik, D. S.; Kikuchi, K.; Hilvert, D. *J. Am. Chem. Soc.* **2000**, *122*, 1022−1029.
(6) Genre-Grandpierre, A.; Tellier, C.; Loirat, M. J.; Blanchard, D.; Hodgson, D. R. W.; Hollfelder, F.; Kirby, A. J. *Bioorg. Med. Chem. Lett.* **1997**, *7*, 2497−2502.
(7) Kennan, A. J.; Whitlock, H. W. *J. Am. Chem. Soc.* **1996**, *118*, 3027−3028.
(8) Perez-Juste, J.; Hollfelder, F.; Kirby, A. J.; Engberts, J. B. F. N. *Org. Lett.* **2000**, *2*, 127−130.
(9) Hollfelder, F.; Kirby, A. J.; Tawfik, D. S. *J. Org. Chem.* **2001**, *66*, 5866−5874.
(10) Shulman, H.; Keinan, E. *Org. Lett.* **2000**, *2*, 3747−3750.

Table 1. Rate Constants for the Uncatalyzed and Catalyzed Decarboxylations of 5-Nitrobenzisoxazoles in Different Catalytic Systems

catalyst	$k_{background}$ (s^{-1})[j]	k_{cat} (s^{-1})
34E4[a]	3.1×10^{-5}	0.66
34E4[b]	2.2×10^{-7}	0.30
BSA[c]	1.6×10^{-3}	2.5
BSA[d]	3.1×10^{-5}	0.017
orphan antibody 4B2[e]	$>3.1 \times 10^{-5}$	0.035
organic host[f]	1.1×10^{-7}	0.00063
coal[g]	6.8×10^{-5}	0.014
synzyme[h]	8.0×10^{-8}	0.045
Bu_4NOAc[i]	1.4×10^{-4} M^{-1}	
Et_3N[i]	8.2×10^{-1} M^{-1}	

[a] 20 °C, 40 mM phosphate buffer containing 100 mM NaCl, pH 7.4, ref 2. [b] 20 °C, 40 mM sodium acetate buffer containing 100 mM NaCl, pH 6.0 (the pK_a of the active site carboxylic acid), ref 2 and this work. [c] 20 °C, 40 mM sodium carbonate buffer containing 100mM NaCl, pH 10.2 (the pK_a of the active site amine), ref 4 and this work. [d] 20 °C, 40 mM phosphate buffer containing 100 mM NaCl, pH 7.4, Reference 4. [e] 30 °C, 1% CH_3CN, 40 mM phosphate buffer containing 100 mM NaCl, pH 7.1, ref 6. The value of $k_{background}$ originally reported in ref 6 is 1.9×10^{-6} s^{-1}, which is inconsistently low and is presumably a misprint. [f] Room temperature, $CDCl_3$, ref 7. [g] 4 °C, 50 mM phosphate buffer containing 2% acetonitrile, pH 7.4, ref 10. [h] 25 °C, 70 mM BisTris buffer, pH 5.9, ref 9. [i] 25° C, H_2O, ref 1d. [j] $k_{background}$ is obtained by extrapolation to zero buffer concentration.

high pH and are less efficient even though the absolute value of k_{cat} in the pH-independent range is higher.

Although many different interpretations have been offered for the catalysis by these diverse materials, the binding of substrate into a relatively nonpolar environment and particularly the desolvation of acetate have usually been thought to be responsible for the rate acceleration. By contrast, the amine-catalyzed reaction is relatively insensitive to solvent polarity, presumably because the uncharged base is not dramatically stabilized by hydrogen bonding. Thus, the reactions involving amine bases, such as polyamines, serum albumins, and synzymes are not easy to explain by medium polarity effects.

Vigorous discussion has broken out about how two types of protein catalysts, (1) tailored catalytic antibodies such as 34E4,[2] and (2) "off-the-shelf" proteins such as serum albumins,[3,4] accelerate this transformation. The two proteins are likely to exploit carboxylate and amine groups as catalytic bases, respectively. Hilvert and Kirby independently determined that serum albumins catalyze the Kemp ring-opening with k_{cat} similar to that found with catalytic antibody 34E4.[3,4] Hilvert identified Lys222 as the catalytic group in bovine serum albumin subdomain II A. There is also a set of positively charged residues that stabilize the phenolate product formed in the reaction.[4] However, Kirby proposed that the low polarity of the interiors of the albumin and 34E4 is the factor responsible for most of the rate acceleration in both cases.[3]

We have studied how these different proteins accelerate this reaction. Kinetic measurements on substituted compounds have been performed to show how specific interactions with nonpolar residues and nonspecific medium effects influence the stability and structure of the transition state. Quantum mechanical calculations of acetate and amine catalyzed reactions in the gas phase and in nonpolar and aqueous solutions have been used to explore the origins of acceleration by nonpolar solvents. The docking and binding of reactants and transition states in the antibody and serum albumin have provided detailed pictures of the origins of antibody and protein catalysis, specifically relative importance to catalysis of polarity and positioning of functional groups in the binding site.

Whether or not proteins can accelerate reactions merely by altering the microenvironment around a substrate and transition state has been the subject of an ongoing debate. Dewar attributed catalysis of chymotrypsin and carboxypeptidase A to the ability of these enzymes to eliminate solvent from the binding pocket and to provide a nonpolar environment for the reaction.[11] He also emphasized the importance of a nonpolar environment for acceleration of various reaction types.[12] On the other hand, Warshel has used thermodynamic arguments to show that desolvation effects alone are unlikely to be the origin of enzyme activity.[13] Although a polar molecule is destabilized by being bound into a nonpolar environment, a free energy penalty must be paid to remove the ionic molecule from water. Warshel proposes that electrostatic interactions between the oriented dipoles of the preorganized protein binding pocket and the substrate generally cause catalysis.[13] In general, Warshel embraces the effectively high polarity of protein binding sites and attributes catalysis to the ideal electrostatic complementarity of protein binding site and transition state.

Although some investigators have advocated pure medium effects ("The medium is the message" in McLuhan's words),[3] others have highlighted contributions of structural effects and specific interactions to catalysis. For example, Bruice emphasizes the ability of a protein to assemble substrates specifically into a geometry suitable for reaction (NACs, near attack conformations) regardless of the polarity of the microenvironment.[14]

Throughout these discussions, confusion has occasionally arisen by the use of different definitions of "medium." The dictionary definition emphasizes more or less homogeneous surroundings: "Any intervening substance through which a force acts on objects at a distance or through which impressions are conveyed to the senses: applied, e.g., to the air, the ether, or any substance considered with regard to its properties as a vehicle of light or sound."[15] This definition of "medium" implies a homogeneous environment. However, the word is often used to indicate specific characteristics of surroundings even when they are heterogeneous. "Microenvironment" is used here as a term to describe the active site of a protein catalyst, especially to convey the heterogeneity that is always a characteristic of a protein interior.

Kinetic Studies. Kemp explored the kinetics of the reactions of substituted benzisoxazoles (BI) with tertiary amines in water.[1] The kinetics follow Brønsted linear free energy relationships (LFERs) over a broad range of reactivity. The slope, β, of a plot of log k vs pK_a of the leaving group, pK_{lg}, provides a measurement of the relationship between the reaction rate and the reaction exothermicity and yields information about the structure and solvation of the transition state (TS).[16] We have measured the rates and β_{lg} values for these eliminations in several solvents and with protein catalysts. These are compared to water as a standard. Table 2 lists the benzisoxazoles studied,

(11) Dewar, M. J. S.; Storch, D. M. *Proc. Natl. Acad. Sci. U.S.A.* **1985**, *82*, 2225−2229.
(12) Dewar, M. J. S.; Healy, E. *Organometallics* **1982**, *1*, 1705−1708.
(13) Warshel, A. *J. Biol. Chem.* **1998**, *273*, 27035−29038.
(14) Bruice, T. C.; Lightstone, F. C. *Acc. Chem. Res.* **1999**, *32*, 127−136.
(15) Oxford English Dictionary, Second Edition, 1989.
(16) Hammond, G. S. *J. Am. Chem. Soc.* **1955**, *77*, 334−338; Leffler, J. E. *Science* **1953**, *117*, 340−341.

Table 2. Kinetic Parameters for the Decomposition of Substituted Benzisoxazoles

benzisoxazole	pK_a phenol	k_{AcO^-,H_2O} (M^{-1} s^{-1})	k_{AcO^-,CH_3CN} (M^{-1} s^{-1})	k_{BuNH_2,H_2O} (M^{-1} s^{-1})	k_{BuNH_2,CH_3CN} (M^{-1} s^{-1})	$(k_{cat}/K_m)_{34E4}$ (M^{-1} s^{-1})	$(k_{cat}/K_m)_{BSA}$ (M^{-1} s^{-1})
5,7-$(NO_2)_2$	0.6	2.76×10^{-3}	759 000			650 000	4530
5,6-$(NO_2)_2$	2.5	1.88×10^{-4}	57 800			3840	457
5-NO_2, 6-Cl	3.6	2.73×10^{-5}	4510	0.116	0.949	22 600	147
5-NO_2	4.1	1.33×10^{-5}	1000	0.0326	0.261	5450	23.9
5-CN	4.7	4.52×10^{-6}		0.0218	0.0603	144	1.81
6-NO_2	5.2	2.47×10^{-6}	104	0.0112	0.0247	0.177	1.52
5,6-Cl_2	5.6	1.52×10^{-6}		0.00854	0.0205	9.64	1.78
6-Cl	6.1		19.4			0.635	0.255
5-Cl	6.4					3.3	0.548
5-F	6.8		1.73			0.659	0.0218
unsubstituted	6.9		0.735			0.155	

[a] Experimental conditions: The second-order rate constants for the acetate and butylamine dependent reactions were determined in water or acetonitrile at 20 °C under pseudo-first order conditions as previously described. The reactions with 34E4 and BSA were performed in 40 mM phosphate, 100 mM NaCl, pH 7.4 and 20 °C.

Table 3. Relative Second Order Rate Constants and Brønsted Coefficients for the Decomposition of Substituted Benzisoxazoles

base/catalyst, medium	k_{rel}[a]	β_{lg}	r^2	no. of points
acetate, H_2O	1	-0.67 ± 0.01	0.998	8
acetate, CH_3CN	7.5×10^7	-0.95 ± 0.05	0.983	8
butylamine, H_2O	2.5×10^3	-0.53 ± 0.07	0.946	5
butylamine, CH_3CN	2.0×10^4	-0.86 ± 0.09	0.967	5
antibody 34E4, H_2O (pH 7.5)	4.1×10^8	-1.48 ± 0.13[b]	0.956	8
BSA, H_2O (pH 7.5)	1.8×10^6	-0.82 ± 0.07	0.946	10

[a] The second-order rate constant (k_{base} or k_{cat}/K_m) for the 5-NO_2 derivative. [b] Excluding 6-nitro, 5,6-dinitro, and 5,7-dinitrobenzisoxazoles, which deviate systematically from the correlation due to comparatively large K_m values (see Figure 2).

along with the pK_a values of the leaving group of the corresponding phenols and the rate constants measured in water and acetonitrile (MeCN) with different bases and catalysts. Table 3 lists the β_{lg} values derived from the plots shown in Figure 2. Excellent LFERs are found for the eliminations promoted by butylamine or acetate as base, in both water and acetonitrile solvents, and with the catalytic antibody 34E4 and bovine serum albumin (BSA) as catalysts.

The β_{lg} values for these correlations vary from -0.53 to -1.48. In each case, the reaction rate increases with decreasing salicylonitrile pK_a, indicating substantial transfer of negative charge to the ether oxygen of the benzisoxazole in the transition state. The reactions involving acetate and butylamine in water have the smallest β_{lg} values; they are least sensitive to the stability of the leaving group. The similarity of the values suggests that the structures and strengths of the base have little influence on the transition state structure and its solvation in water. The change to acetonitrile as solvent causes a 10^8 acceleration with acetate as base, but only a 10-fold effect with the amine base. Despite dramatically different effects on the rates with different bases, the Brønsted β_{lg} values are -0.9 to -1.0 for both acetate and butylamine in acetonitrile. The values are close to -1, so that the effect of leaving group stability is strongly felt in the transition state. However, the aqueous pK_a values are used for this correlation, while one would expect a larger spread of pK_a values for a related nonpolar solvent. In the lower dielectric environment, there is greater sensitivity to charge development at oxygen.

These results can be compared and contrasted with those obtained with the protein catalysts BSA and antibody 34E4. BSA accepts a wide variety of mono- and di-substituted benzisoxazoles as substrates (Table 2), and the Brønsted β_{lg}

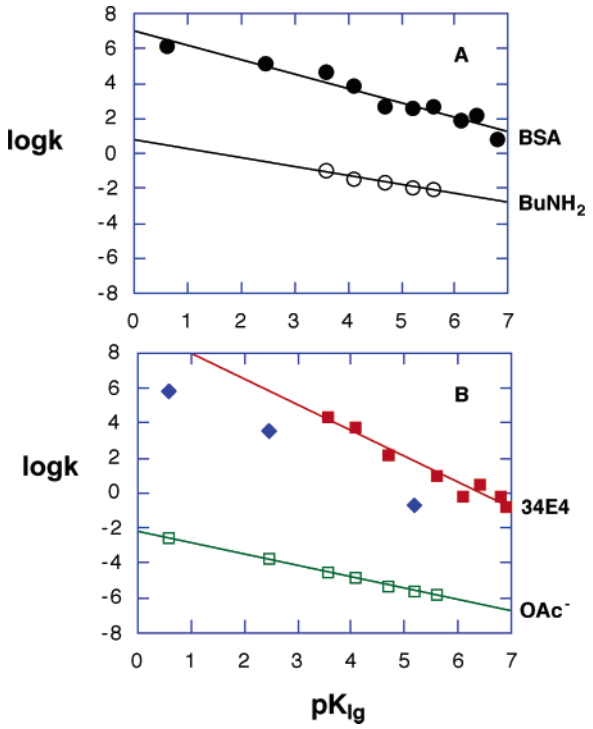

Figure 2. (A) Brønsted plot for the aqueous reaction of substituted benzisoxazoles with $BuNH_2$ (○) or with BSA (●). The apparent second-order rate constant $(k_{cat}/K_m)_{BSA}$ obtained at pH 7.4 was extrapolated to its maximum value using the known pH-dependence of the BSA-catalyzed reaction. (B) Brønsted plot for the aqueous reactions of BI with acetate (□) or 34E4 (■). The reactions of 34E4 with 5,7-dinitro-, 5,6-dinitro-, and 6-nitrobenzisoxazole (◆) deviate systematically from the correlation relating the other eight substrates.

value correlating these reaction rates is similar to that obtained with butylamine in acetonitrile. This suggests that the protein binding pocket that contains Lys222, the likely catalytic base,[9,17] presents a microenvironment to the developing phenoxide that is similar to that of acetonitrile.

Antibody 34E4 likewise accepts a wide range of substituted benzisoxazoles as substrates, but as shown in Figure 2, the reaction rate is unusually sensitive to leaving group effects. Eight of the eleven substrates tested are correlated with $\beta_{lg} = -1.5$, which is much larger than any of the other Brønsted coefficients. In this environment, the elimination rates respond more to substituent effects than aqueous pK values do. This mostly likely

(17) Carter, D. C.; Ho, J. X. *Adv. Prot. Chem.* **1994**, *45*, 153−203.

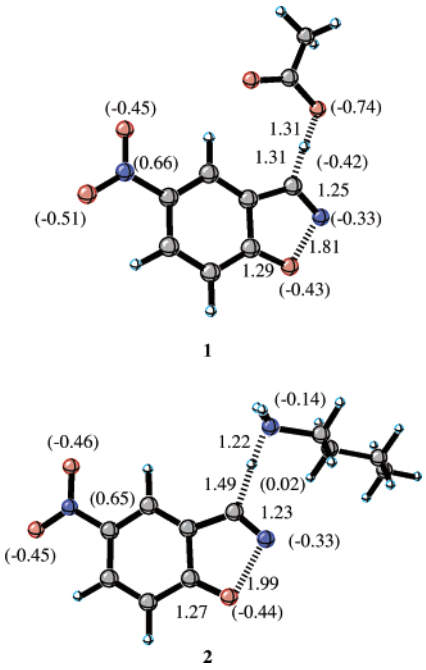

Figure 3. Computed transition states for reaction of acetate and butylamine with 4-nitrobenzisoxazole. Relevant bond lengths and charges are shown.

arises from the enhanced basicity of the phenoxide leaving group in a relatively nonpolar environment, which leads to a larger spread in phenoxide pK values than in water or acetonitrile and a β value greater than -1.

The Brønsted plot for k_{cat} similarly yields $\beta_{lg} = -1.5$ ($r^2 = 0.97$) as a consequence of the similar K_m values (100−200 μM) exhibited by these substrates. Benzisoxazoles containing a nitro substituent at the 6- or 7-position deviate negatively from the correlation in 34E4 shown in Figure 2 and appear to lie along a line that is roughly parallel to that through the data for the other substrates. These substrates have substantially larger K_m values than the others, suggesting that they adopt a different binding mode at the active site. However, the large kinetic isotope effect ($V/K^D = 5.7$) measured for the most reactive compound, 5,7-dinitrobenzisoxazole ($k_{cat} = 660\ s^{-1}$, $K_m = 1.0$ mM), shows that CH bond-breaking is still rate limiting for these substrates. The large β value for 34E4 indicates that the developing negative charge is relatively destabilized by the environment so that the substituent effects are very large, and reflect the very large role of substituent, rather than microenvironment, on charge stabilization. The results suggest that the local environment of 34E4 around the leaving group is effectively less polar than acetonitrile.

Quantum Mechanical Studies of the Base-Promoted Benzisoxazole Ring-Opening. Quantum mechanical calculations[18] and solvation energy estimations[19−22] were performed as described in the Experimental Section. The optimized geometries of the two transition states with acetate and butylamine as bases in the gas phase are shown in Figure 3. The proton is more completely transferred in the amine reaction, but the C−(H)−O and C−(H)−N distances are similar, at 2.62 and 2.71 Å, respectively. The lengths of the breaking N−O bonds in the five-membered ring are 1.81 and 1.99 Å in the two transition states, respectively. The charges on nitrogen (−0.33) and oxygen (−0.44) of the cleaving benzisoxazole ring are almost identical.

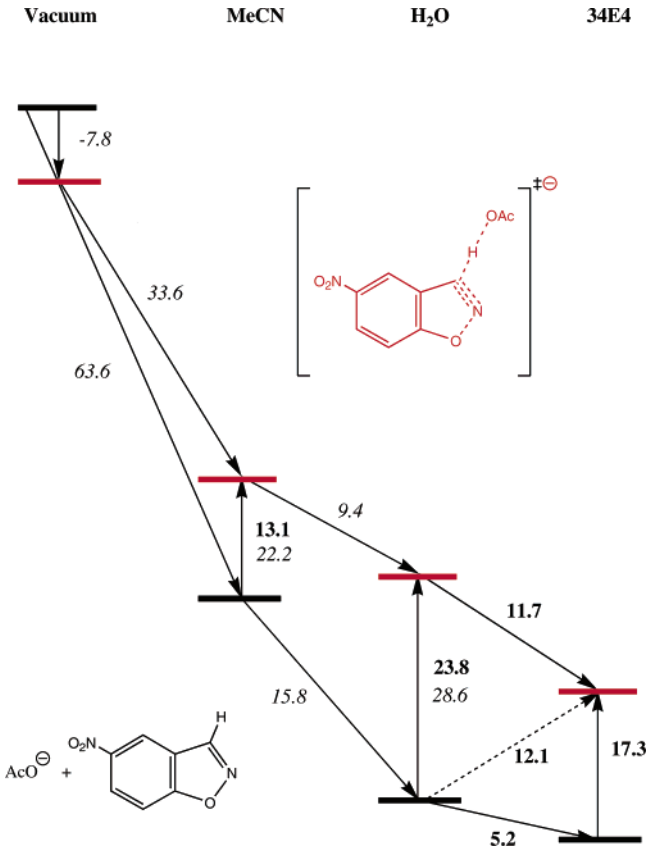

Figure 4. Free energy (ΔG) diagrams for reactions of acetate with 4-nitrobenzisoxazole in gas phase, acetonitrile, water, and antibody 34E4. Numbers in bold face are experimental values and those in italics are the averaged calculated values based on PCM and CPCM models.

Therefore, the E2 type geometry of the Kemp ring-opening does not change significantly with different bases.

The calculated activation barrier in the gas phase is −7.8 kcal/mol for the acetate catalyzed reaction, because there is an ion−molecule complex between the ionic reactant, acetate, and benzisoxazole, which is lower in energy than the reactants and the transition state for elimination. The conversion of this complex to the transition state has a normal positive activation barrier in solutions.

Solvation Energy Calculations. The calculated solvation free energies of acetate are all within 3 kcal/mol of the experimental aqueous solvation free energy of acetate (−77 kcal/mol).[23] The free energies of reactants and transition states in solvents are sums of the single point solvation free energies based on the

(18) Gaussian 98, Revision A.9, Frisch, M. J.; Trucks, G. W.; Schlegel, H. B.; Scuseria, G. E.; Robb, M. A.; Cheeseman, J. R.; Zakrzewski, V. G.; Montgomery, J. A.; Stratmann, Jr., R. E.; Burant, J. C.; Dapprich, S.; Millam, J. M.; Daniels, A. D.; Kudin, K. N.; Strain, M. C.; Farkas, O.; Tomasi, J.; Barone, V.; Cossi, M.; Cammi, R.; Mennucci, B.; Pomelli, C.; Adamo, C.; Clifford, S.; Ochterski, J.; Petersson, G. A.; Ayala, P. Y.; Cui, Q.; Morokuma, K.; Malick, D. K.; Rabuck, A. D.; Raghavachari, K.; Foresman, J. B.; Cioslowski, J.; Ortiz, J. V.; Baboul, A. G.; Stefanov, B. B.; Liu, G.; Liashenko, A.; Piskorz, P.; Komaromi, I.; Gomperts, R.; Martin, R. L.; Fox, D. J.; Keith, T.; Al-Laham, M. A.; Peng, C. Y.; Nanayakkara, A.; Challacombe, M.; Gill, P. M. W.; Johnson, B.; Chen, W.; Wong, M. W.; Andres, J. L.; Gonzalez, C.; Head-Gordon, M.; Replogle, E. S.; Pople, J. A. Gaussian, Inc., Pittsburgh, PA, 1998.
(19) Barone, V.; Cossi, M.; Tomasi, J. *J. Comput. Chem.* **1998**, *19*, 404−417.
(20) Miertus, S.; Scrocco, E.; Tomasi, J. *Chem. Phys.* **1981**, *55*, 117−129.
(21) JAGUAR (Schrödinger, Inc., Portland, OR) Version 4.0, 2000.
(22) "AMSOL 6.5", Hawkins, G. D.; Giesen, D. J.; Lynch, G. C.; Chambers, C. C.; Rossi, I.; Storer, J. W.; Rinaldi, D.; Liotard, D. A.; Cramer, C. J.; Truhlar, D. G.
(23) Pearson, R. G. *J. Am. Chem. Soc.* **1986**, *108*, 6109−6114.

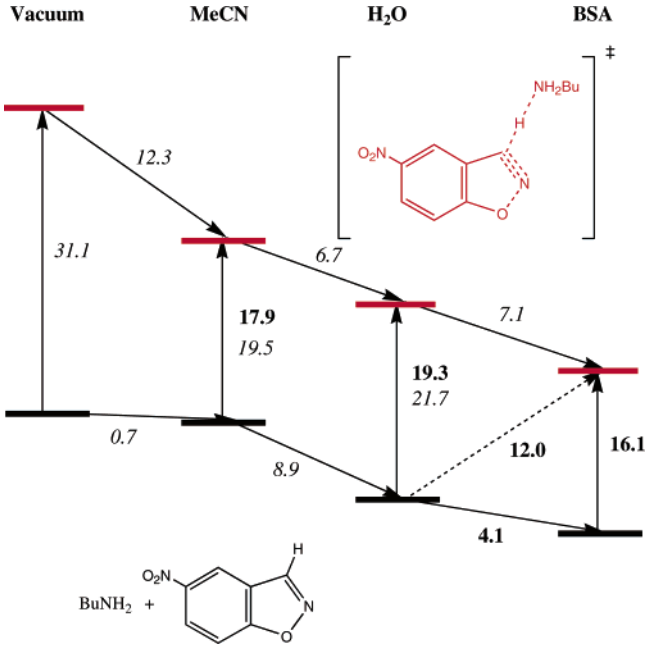

Figure 5. Free energy (ΔG) diagrams for reactions of butylamine with 4-nitrobenzisoxazole in the gas phase, acetonitrile, water and BSA. Numbers in bold face are experimental values and those in italics are the averaged calculated values based on PCM and CPCM models.

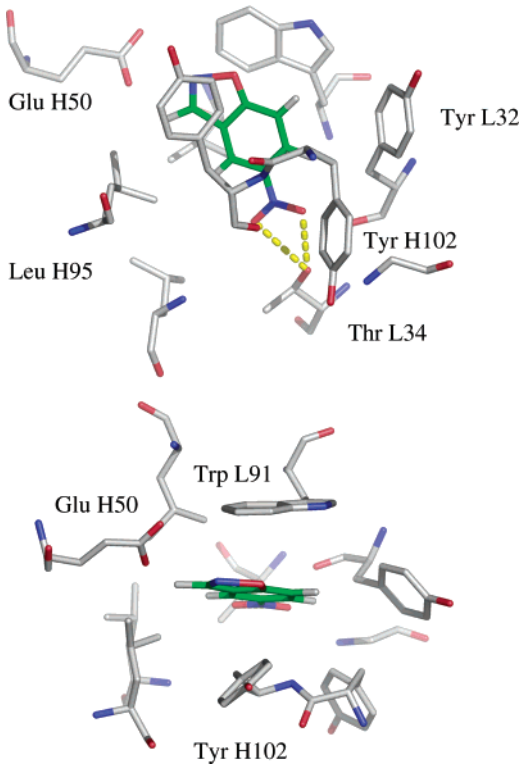

Figure 6. Docked binding mode of TS minus AcO^- in the 34E4 binding site. (a) Side view (b) Top view.

gas-phase geometries, and the relevant free energies in the gas phase. All of the methods overestimate the activation barriers in both water and MeCN. The CPCM model shows a change in the activation energy (7 kcal/mol) from water to acetonitrile which is closes to the experimental value (11 kcal/mol).

Figure 4 summarizes the energetics of acetate- and 34E4-promoted eliminations. CPCM calculations predict that acetate and benzisoxazole are stabilized by a total of 63.6 kcal/mol in acetonitrile, while the transition state **1** is solvated by only 33.6 kcal/mol. Because the reactants are stabilized much more than the transition state, the activation barrier changes from −7.8 kcal/mol in the gas phase to 22.2 kcal/mol in acetonitrile. The reactants and transition state are stabilized further by 15.8 and 9.4 kcal/mol, respectively, when changing the solvent from acetonitrile to water. The new activation barrier is calculated to be 28.6 kcal/mol, which is 6.4 kcal/mol higher than in acetonitrile, experiment shows an even larger activation barrier increase of 10.7 kcal/mol. Larger basis sets are likely to improve agreement with experiment. For the acetate-promoted process, the gas phase activation barrier (and consequently all the others) is decreased by 2 kcal/mol.

For the amine-catalyzed reaction, summarized in Figure 5, the activation barrier in the gas phase is 31.1 kcal/mol due to the difficulty of charge separation in the gas phase. The reactants are barely solvated by acetonitrile (0.7 kcal/mol), while the transition state is stabilized by 12.3 kcal/mol due to its high polarity. This leads to a smaller activation barrier (19.5 kcal/mol) in acetonitrile than in the gas phase. The additional changes of solvation free energies upon transfer from acetonitrile to water for reactants and transition state **2** are 8.9 and 6.7 kcal/mol, respectively. The resulting activation barrier in water (21.7 kcal/mol) is slightly higher than in acetonitrile, because the reactants are stabilized more than transition state. These calculations show good agreement with experiment for both acetonitrile and water.

Acetate has an experimental pK_a value of 4.8 in water and 22.3 in acetonitrile,[24] and this large change is reflected in the large rate acceleration of the elimination in acetonitrile. However, experiment and calculation show that there is only a 2∼3 kcal/mol barrier change for the amine-catalyzed reaction. The small activation barrier change in the amine-catalyzed reaction is related to the smaller pK fluctuation from 10.8 in water to 18.3 in acetonitrile.[23]

Transfer of Substrates and Transition States from Water to Protein. The binding energies for reactants, estimated from measured K_m values, are 5.2 and 4.1 kcal/mol for 34E4 and BSA, respectively. The calculated free energy corresponding to k_{cat}/K_m is 12.1 kcal/mol for the reaction catalyzed by 34E4 and 12.0 kcal/mol for BSA. These results are also shown in Figures 4 and 5. According to the thermodynamic cycle, 34E4 and BSA stabilize the transition states by 11.7 and 7.1 kcal/mol relative to water, respectively. In acetate- and amine-catalyzed reactions, both the reactants and transition states are stabilized upon proceeding along the series from vacuum to acetonitrile, water, and protein. The protein catalysis occurs by lowering the free energy of the transition state in the protein complex more than the substrate in the protein complex. A similar trend was also found in our study of another solvent sensitive reaction, the antibody-catalyzed Kemp decarboxylation.[25]

Docking Studies with 34E4. To explore in detail the mechanism of antibody catalysis, the substrate and transition state were docked into the binding sites of 34E4. In the absence of a crystal structure for 34E4, we used a homology-based model

(24) Kolthoff, I. M.; Chantoon, M. K.; Bhowmik, S. *J. Am. Chem. Soc.* **1968**, *90*, 23−28.
(25) Ujaque, G.; Tantillo, D.; Hu, Y.; Houk, K.; Hotta, K.; Hilvert, D. *J. Comput. Chem.* **2003**, *24*, 98−110.

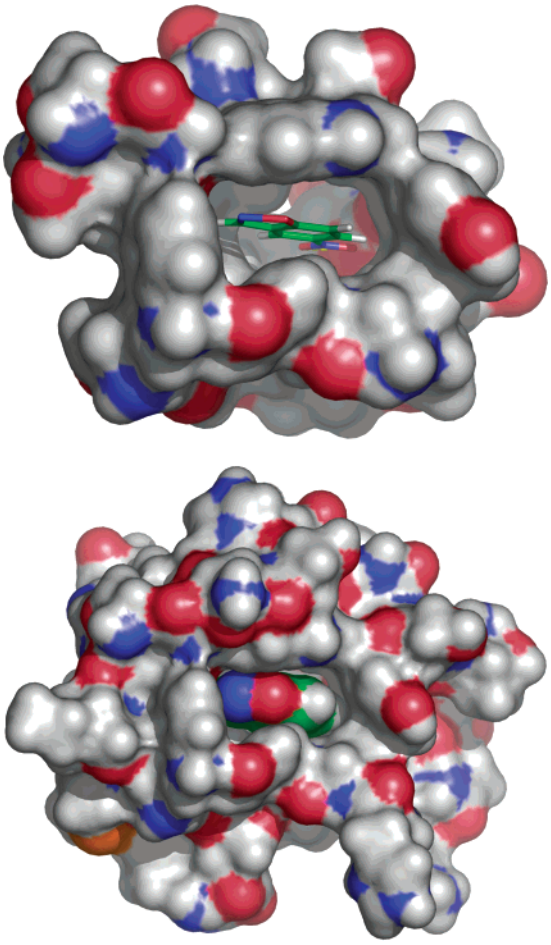

Figure 7. 34E4 surface including residues within 5 Å (top) and 8 Å (bottom) of the docked transition state.

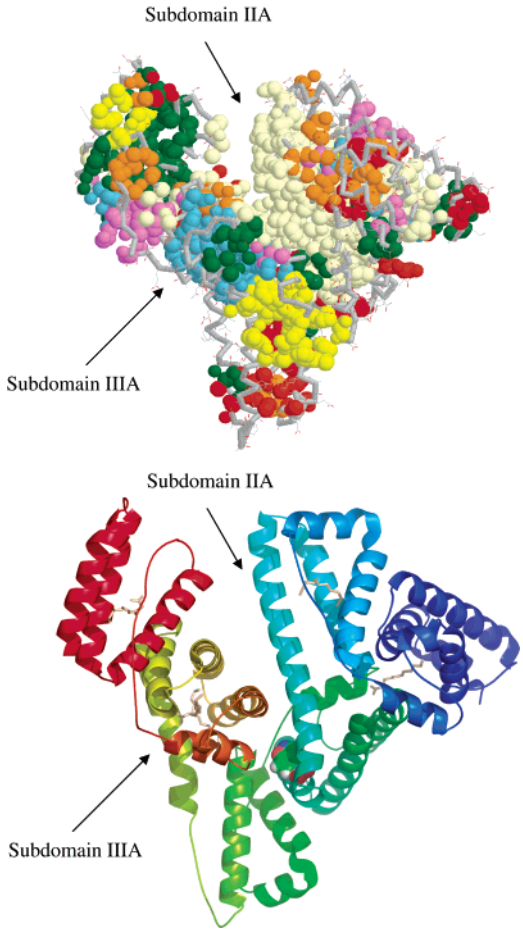

Figure 8. Human serum albumin. (a) Binding pockets and cavities calculated by CAST (b) The docked transition state and the myristic acid inhibitor.

based on the sequence of 34E4 obtained here (see Experimental Section). Figure 6 shows the best transition state docking mode for the acetate-catalyzed reaction in 34E4 in both side and top views. It has an estimated free energy of binding of −7 kcal/mol, according to the AUTODOCK free energy scoring function. In the vicinity of the benzisoxazole moiety, there are mostly hydrophobic residues. The nitro group is buried in the bottom of the 34E4 binding pocket, and forms two hydrogen bonds with Thr L34. The tight steric fit of the substrate within the pocket also suggests why substituents at the 6-position influence substrate binding (K_m) to a considerable extent in kinetic experiments (Table 2). Near the entrance to the binding site, the benzisoxazole transition moiety is surrounded by Tyr L32, Trp L91, Tyr H102, Tyr H103, and Glu H50, all of which are within 5 Å of the transition state. A potential base, Glu H50 is placed perfectly to deprotonate the benzisoxazole and initiate ring-opening. The distance of the nearest carboxylate oxygen from the transferring proton is 2.5 Å. The proposed role in catalysis is consistent with preliminary mutagenesis results showing that activity is abolished when GluH50 is substituted with glutamine.[27]

Figure 7 shows the solvent accessible surfaces of the 34E4 binding pocket including residues within 5 Å (top) or 8 Å (bottom) of the transition state. The transition state is trapped deeply inside the complementary binding pocket, which has a very narrow entrance formed by several hydrophobic residues. The second view shows that the transition state in 3D representation is in relatively tight contact with the surroundings. The region of negative electrostatic potential (red) is concentrated on the Glu H50 side, near where the proton of the benzisoxazole is located.

Antibody 34E4 provides a preorganized microenvironment made of hydrophobic and polar residues around the reaction center, with the basic site oriented for deprotonation of the benzisoxazole. The oxygen of the benzisoxazole ring is situated so as to be solvated by external water as it is transformed into cyanophenoxide.

Serum Albumin Catalysis. Serum albumins are ubiquitous proteins in the blood stream; albumins bind various small molecules in multiple binding sites. Hilvert and Kirby's experiment show that BSA and human serum albumin (HSA) have similar effects on the benzisoxazole elimination, and there is a binding site with lysine group present in each case.[5] Because the BSA crystal structure is unavailable, we used the HSA crystal structure for the docking study.

Two binding pockets with the highest CAST score (see Experimental Section) are the most likely binding sites (Figure 8). Subdomains IIA and IIIA, shown as light yellow and light blue, are also the two sites that have been proposed to bind small heterocyclic substrates such as warfarin experimen-

(26) Morris, G. M.; Goodsell, D. S.; Halliday, R. S.; Huey, R.; Hart, W. E.; Belew, R. K.; Olson, A. J. *J. Comput. Chem.* **1998**, *19*, 1639−1662.
(27) Seebeck, F., unpublished results.

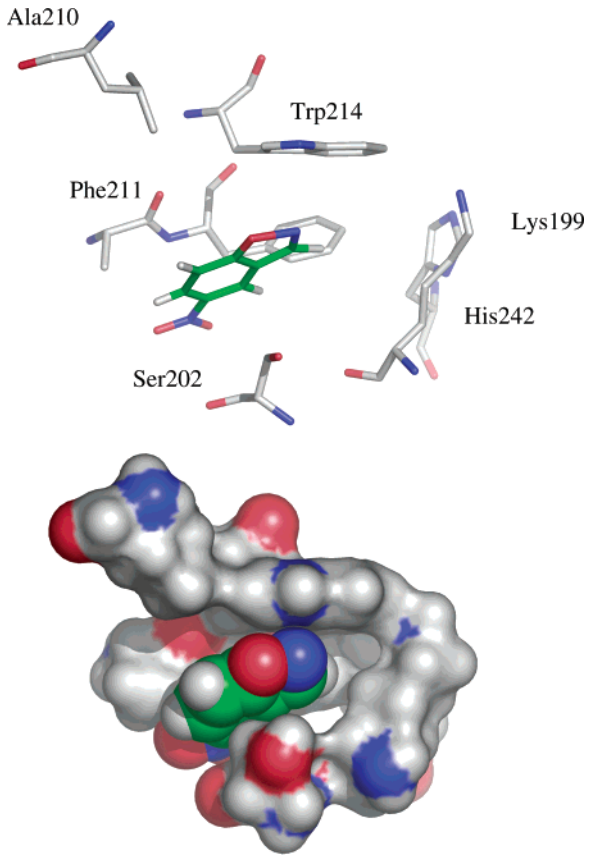

Figure 9. Transition state moiety in HSA subdomain IIA. (a) Residues within 5 Å of the transition state (b) Surface representation of residues within 5 Å of the transition state.

tally.[29,30] The five myristic acids determined from the same crystal structure are shown in the second view (Figure 8b). Although there are lysine residues on the HSA surface, none of them can be considered as effective catalytic bases because of their high pK_a values on the protein surface. There is one lysine in subdomain IIA and no lysine residues inside the subdomain IIIA. Consequently, we focused our attention on the IIA subdomain.

Autodock produced a binding mode that is shown in Figures 9 and 10. The average estimated free energy of binding is −6 kcal/mol. Figure 9 shows stick and space-filling renderings of the protein with the transition state surrounded by residues in the cleft of subdomain IIA within 5 Å. The pocket has mainly nonpolar residues including Trp 214, Ala 219, Phe 211, Ser 202, His 242, and the putative base, Lys 199. The latter is 5.4 Å away from the transferring hydrogen. The only tryptophan in albumin, Trp214, has $\pi-\pi$ interactions with benzisoxazole aromatic ring. There is barely enough room for the transition state to stay in such a steep and narrow pocket. This can be seen from the comparison of 5 Å (Figure 9b) and 8 Å (Figure 10) surfaces. The transition state resides in the concave part of the binding pocket. Such a binding mode is not easily accessible from outside without conformational changes of the albumin upon binding the ligand. Lys 195 is located in subdomain IIA

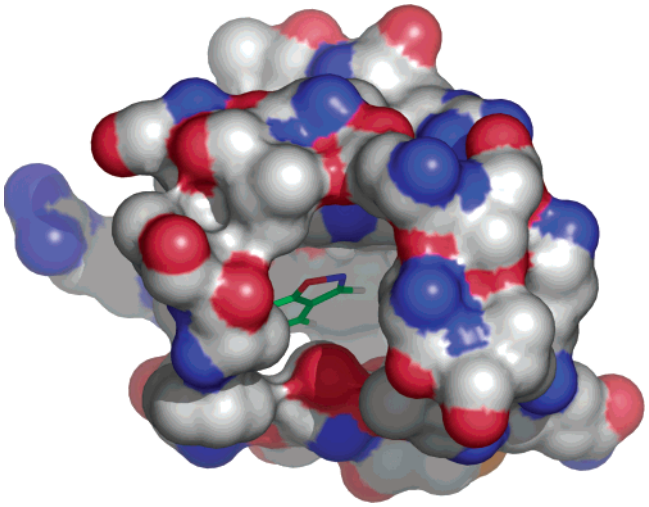

Figure 10. Surface representation of residues within 8 Å of the transition state.

next to Lys 199. The protonation states of these two lysine groups have been studied both experimentally and theoretically. The combination of a neutral Lys 199 and protonated Lys 195 is the most favored one since they can form a hydrogen bond with water.[31] Experiments show that Lys 199 has a low pK_a (∼8).[32] Therefore, we postulate that Lys 199 is the catalytic group in human serum albumin, whereas Lys222 is the catalytic group in bovine serum albumin. Experiments also indicate that HSA loses most of its catalytic ability upon Lys199 modification,[5] confirming the predictions from docking experiments.

Conclusion

The mechanisms of catalysis of the Kemp elimination have been elucidated for reactions occurring in two proteins, and the rates have been computed in aqueous and nonpolar solvents. Antibody 34E4 catalyzes this reaction by the alignment of catalytic base Glu H50 and substrate benzisoxazole within a relatively nonpolar pocket. Similarly, HSA has a deep nonpolar pocket at subdomain IIA with Lys 199 that can deprotonate 5-nitrobenzisoxazole.

An analogy between enzymes and organic solvents is often made, but the heterogeneous microenvironment of a protein pocket is clearly different from free solvent molecules in that its fixed structure can be tuned to interact with and stabilize disparate components of a reacting molecule. The efficiency of these biological catalysts derives from having a catalytic base geometrically positioned in a generally nonpolar active site, a consequence of successful hapten design in 34E4, but serendipitous in albumin. From the evolutionary perspective, there is no fundamental difference between our specific residue positioning argument and Kirby's more recent proposal of a specific medium effect.[9,33] The specific medium effect involves dispersion and electrostatic interactions with the transition state, which is a necessary outcome of the specific group positioning. The ultimate biological catalyst must utilize a perfect match

(28) (a) Liang, J.; Edelsbrunner, H.; Woodward, C. *Protein Science* **1998**, *7*, 1884−1897. (b) Liang, J.; Edelsbrunner, H.; Fu, P.; Sudhakar, P. V.; Subramaniam, S. *Proteins* **1998**, *33*, 1−17.
(29) Bhattacharya, A. A.; Grune, T.; Curry, S. *J. Mol. Biol.* **2000**, *303*, 721−732.
(30) Zaton, A. M. L.; Villamor, J. P. *Chem.-Biol. Interact* **2000**, *124*, 1−11.
(31) (a) Diaz, N.; Suarez, D.; Sordo, T. L.; Merz, Jr., K. M. *J. Med. Chem.* **2001**, *44*, 250−260. (b) Bhattacharya, A. A.; Petitpas, I.; Twine, S.; East, M.; Curry, S. *J. Biol. Chem.* **2001**, *276*, 22 804−809.
(32) (a) Gerig, J. T.; Reiheimer, J. D. *J. Am. Chem. Soc.* **1975**, *97*, 168−173. (b) Gerig, J. T.; Katz, K. E.; Reinheimer, J. D. *Biochim. Biophys. Acta* **1978**, *534*, 196−209.
(33) Hollfelder, F.; Kirby, A. J.; Tawfik, D. S. *J. Am. Chem. Soc.* **1997**, *119*, 9578−9579.

between the catalytic group and the transition state plus an elaborate active site made of polar and nonpolar groups, which provides favorable interactions with the transition state including electrostatics, solvation and other factors.[34] The most important feature for catalysis is the assembly of catalytic functionality, here the basic site, with appropriate orientation and reactivity. Of course catalysts that accidentally have an appropriate environment do exist, such as albumins in this case.

Catalytic antibodies represent a successful effort to biological catalyst design for nonbiological reactions. The problems in such design and execution are known[5] to be difficult but not insoluble.[36,37] A remaining challenge is how to use the programmable nature of the antibody pocket along with medium effects to act in concert with other active site parameters. Careful design by increasing the strength of the catalytic base through desolvation and by providing specific stabilizing interactions with the leaving group such as forming hydrogen bonds with phenoxide, should lead to better catalysts for such a solvent sensitive reaction.[38]

Experimental Section

Synthesis of Substituted Benzisoxazoles. Unsubstituted benzisoxazole and the 5-nitro-, 6-nitro-, 5,7-dinitro-, 5-chloro-, and 6-chloro-substituted derivatives were prepared according to the literature.[1a,39] 4-Cyano- and 4-fluorosalicylaldehyde were prepared from the corresponding phenols by a Duff reaction;[40] 4,5-dichlorosalicylaldehyde was prepared by a Reimer−Tiemann reaction.[41] The substituted salicylaldehydes were converted to benzisoxazoles by a standard literature procedure.[39b]

5-Cyanobenzisoxazole. ^{1}H NMR (300 MHz, $CDCl_3$) δ 7.76 (q, 1H), 7.84 (q, 1H), 8.16 (d, 1H), 8.83 (d, 1 H). MS FABM$^+$ 145 (M^++H^+). mp 245 °C (decomp.).

5,6-Dichlorobenzisoxazole. ^{1}H NMR (300 MHz, $CDCl_3$) δ 7.80 (d, 1H), 7.85 (s, 1H), 8.68 (d, 1H). MS FABM$^+$ 187/189 (M^++H^+), 210/212 (M^++Na^+). mp 92 °C (sub.).

5-Fluorobenzisoxazole. ^{1}H NMR (300 MHz, $CDCl_3$) δ 7.32 (q, 1H), 7.38 (q, 1H), 7.59 (q, 1H), 8.7 (d, 1 H). MS FABM$^+$ 139 (M^++H^+). mp 68 °C (sub.).

5,6-Dinitrobenzisoxazole. 6-Nitrobenzisoxazole (200 mg) was dissolved in ice-cooled cH_2SO_4 (1.6 mL). Fuming nitric acid (200 μl) was added dropwise, and the reaction mixture was heated at 80 °C for 30 min. The starting material was completely consumed. The reaction mixture was poured onto ice and then extracted immediately with methylene chloride. The organic layer was dried and purified by silica gel chromatography using methylenechloride as eluent to give 142 mg of the desired product in 56% yield. ^{1}H NMR (300 MHz, $CDCl_3$) δ 8.17 (q, 1H), 8.52 (d, 1H), 9.15 (d, 1H). MS FABM$^+$ 210 (M^++H^+). mp 112 °C.

5-Nitro-6-chlorobenzisoxazole. 6-Chlorobenzisoxazole was nitrated at the 5-position by the same method used to prepare 5,6-dinitrobenzisoxazole in 62% yield. ^{1}H NMR (300 MHz, $CDCl_3$) δ 7.88 (d, 1H), 8.36 (d, 1H), 8.86 (d, 1H). MS FABM$^+$ 198/200 (M^++H^+). mp 106 °C.

Kinetic Analyses. All kinetic experiments were performed at 20 °C. Fast reactions were measured by stopped flow techniques. The reactions were initiated by adding the benzisoxazole substrate to the reaction mixture and product formation was monitored spectrophotometrically at the following wavelengths: 5,7-dinitro (352 nm), 5,6-dinitro (380 nm), 5-nitro-6-chloro (380 nm), 5-nitro (380 nm), 5-cyano (324 nm), 6-nitro (404 nm), 5,6-dichloro (342 nm), 6-chloro (329 nm), 5-chloro (339 nm), 5-fluoro (338 nm), and unsubstituted (325 nm). Extinction coefficients were measured for each compound under the reaction conditions. The second-order rate constants for the acetate and butylamine-dependent reactions were determined in water or MeCN at 20 °C. Pseudo-first-order rate constants were plotted against acetate or butylamine concentration, and the slope of these plots gave the second-order rate constant for the base-catalyzed reaction. The reactions with 34E4 and BSA were performed in 40 mM phosphate, 100 mM NaCl, pH 7.4 and 20 °C. Initial velocities were calculated by standard linear-regression analysis using the initial linear portion of absorbance vs time plots and were corrected for background activity. The k_{cat} and K_m values were calculated by fitting the kinetic data to the Michaelis−Menten equation using the program KaleidaGraph. Two percent acetonitrile was used to dissolve the substrate for all reactions in aqueous medium. Crystallized BSA, treated to remove bound lipids, was purchased from Sigma and used without further purification; 34E4 was isolated and purified as previously described.

Cloning of the Antibody Genes. Poly (A)$^+$ mRNA was isolated from the hybridoma producing antibody 34E4.[2] A cDNA library was constructed with the Great Lengths cDNA synthesis kit (Clontech). The V_L and V_H genes were cloned using the polymerase chain reaction with the following primers: V_L sense, GTACATTT*GCTCTTC*GGTTCACAGGCTGTTGTGACTCAGGAA (the *Sac* I restriction site is in italics); V_L anti-sense, ATGAGTTTTTGTTCT*GCGGCCGC*CTTGGGCTGACCTAGGACAGT (*Not* I); V_H sense AGGTCCAGCTG*CTCGAG*TCTGG (*Xho* I); V_H anti-sense GTTCTG*ACTAGT*GGGCACTCTGGGCTC (*Spe* I). The amplified fragments were purified, cloned into appropriate sites in the vector p4xH-M13[42] and sequenced. The resulting expression plasmid, p4xH-34E4, allows production of 34E4 as a chimeric murine-human Fab fragment in which the V_L and V_H segments of the catalytic antibody are fused to human Cκ and gamma C_H1 regions, respectively.[42]

The antibody sequences for the variable segments of 34E4 are given in Chart 1.

Construction of a Homology Model. A search of the structure database identified antibodies HC19 (1gig.pdb)[43] and J539 (2fbj.pdb)[44] as having the highest sequence similarity to the 34E4 V_L and V_H domains, respectively. Because HC19 and 34E4 have CDR H3 loops that are the same length and that possess reasonable sequence similarity (28.6%), modeling of the V_L-V_H interface[45] is facilitated. A least-squares fit of the V_H domains of HC19 and J539, minus the CDR H3 loop, allowed overlay of the two molecules with a rmsd. of 1.40 Å for all Cα atoms except those of the CDR L1 (residues L24 to L34) and H3 (residues H95 to H102). In this overlay, the V_H domains of the two antibodies were superimposed with rmsd. of 0.88 Å for all non-CDR H3 Cα atoms, whereas the V_L domains were overlaid with rmsd. of 1.37 Å for all non-CDR L1 Cα atoms. In particular, the residues near the V_L/V_H interface from the two molecules, namely residues L42-L46, L94-L100, H43-H50, H58-H61, and H103-H105 (27 residues in total), coincided with each other with rmsd. of 0.87 Å for all Cα atoms. Accordingly, visual inspection of the interface between the HC19 V_L and J539 V_H domains revealed that no significant steric interference was introduced by the way the two domains were put together. After

(34) Houk, K. N.; Leach. A. G.; Kim, S. P.; Zhang, X. *Angew Chem., Int. Ed.* **2003**, *42*, 4872−4897.
(35) Zhang, X.; Houk, K. N., submitted for publication.
(36) Tantillo, D. J.; Houk, K. N. *J. Org. Chem.* **1999**, *64*, 3066−3076.
(37) Barbany, M.; Gutierrez-de-Teran, H.; Sanz, F.; Villa-Freixa, J.; Warshel, A. *ChemBioChem* **2003**, *4*, 277−285.
(38) Parker, A. J. *Chem. Rev.* **1969**, *69*, 1−32.
(39) (a) Kemp, D. S.; Woodward R. B. *Tetrahedron* **1965**, *21*, 3019−3035. (b) Casey, M. L.; Kemp, D. S.; Paul, K. G.; Cox, D. D. *J. Org. Chem.* **1973**, *38*, 2294−2301.
(40) Suzuki, Y.; Takahashi, H. *Chem. Pharm. Bull.* **1983**, *31*, 1751−1753.
(41) Postmus, C.; Kaye, I. A.; Craig, C. A.; Matthews, R. S. *J. Org. Chem.* **1964**, *29*, 2693−2698.
(42) Ulrich, H. D., Patten, P. A., Yang, P. L., Romesberg, F. E., & Schultz, P. G. *Proc. Natl. Acad. Sci. U.S.A.* **1995**, *92*, 11 907−11 911.
(43) Bizebard, T.; Daniels, R.; Kahn, R.; Golinellipimpaneau, B.; Skehel, J. J.; Knossow, M. *Acta Crystallog.* **1994**, *D50*, 768−777.
(44) Suh, S. W.; Bhat, T. N.; Navia, M. A.; Cohen, G. H.; Rao, D. N.; Rudikoff, S.; Davies, D. R. *Proteins: Struct. Funct. Genet.* **1986**, *1*, 74−80.
(45) Stanfield, R. L.; Takimoto-Kamimura, M., Rini, J. M.; Profy, A. T.; Wilson, I. A. *Structure* **1993**, *1*, 83−93.

Chart 1

34E4 light chain variable domain

1	2	3	4	5	6	7	8	9	10	11	12
gln	ala	val	val	thr	gln	glu	ser	ala	- - -	leu	thr
13	14	15	16	17	18	19	20	21	22	23	**24**
thr	ser	pro	gly	glu	thr	val	thr	leu	thr	cys	arg
25	**26**	**27**	**27A**	**27B**	**27C**	**28**	**29**	**30**	**31**	**32**	**33**
ser	ser	ser	gly	ala	val	thr	thr	ser	asn	tyr	ala
34	35	36	37	38	39	40	41	42	43	44	45
thr	trp	val	gln	glu	lys	pro	asp	his	leu	phe	thr
46	47	48	49	**50**	**51**	**52**	**53**	**54**	**55**	**56**	57
gly	leu	ile	gly	gly	thr	asn	lys	arg	ala	pro	gly
58	59	60	61	62	63	64	65	66	67	68	69
val	pro	ala	arg	phe	ser	gly	ser	leu	ile	gly	asp
70	71	72	73	74	75	76	77	78	79	80	81
arg	ala	ala	leu	thr	ile	thr	gly	ala	gln	thr	glu
82	83	84	85	86	87	88	**89**	**90**	**91**	**92**	**93**
asp	glu	ala	ile	tyr	phe	cys	ala	leu	trp	asn	ser
94	**95**	**96**	**97**	98	99	100	101	102	103	104	105
asn	his	leu	val	phe	gly	gly	gly	thr	lys	leu	thr
106	106A	107	108	109	110						
val	leu	gly	gln	pro	(lys)*						

34E4 heavy chain variable domain

1	2	3	4	5	6	7	8	9	10	11	12
(glu)	val*	(lys)*	leu	leu	glu	ser	gly	gly	gly	leu	ala
13	14	15	16	17	18	19	20	21	22	23	24
gln	pro	gly	gly	ser	leu	lys	leu	ser	cys	ala	ala
25	26	27	28	29	30	**31**	**32**	**33**	**34**	**35**	36
ser	gly	phe	asp	phe	arg	arg	tyr	trp	met	thr	trp
37	38	39	40	41	42	43	44	45	46	47	48
val	arg	gln	ala	pro	gly	lys	gly	leu	glu	trp	ile
49	**50**	**51**	**52**	**52A**	**53**	**54**	**55**	**56**	**57**	**58**	**59**
gly	glu	ile	asn	pro	asp	ser	arg	thr	ile	asn	tyr
60	**61**	**62**	**63**	**64**	**65**	66	67	68	69	70	71
met	pro	ser	leu	lys	asp	lys	phe	ile	ile	ser	arg
72	73	74	75	76	77	78	79	80	81	82	82A
asp	asn	ala	lys	asn	ser	leu	tyr	leu	gln	leu	ser
82B	82C	83	84	85	86	87	88	89	90	91	92
arg	leu	arg	ser	glu	asp	ser	ala	leu	tyr	tyr	cys
93	94	**95**	**96**	**97**	**98**	**99**	**100**	**100A**	**B**	**C**	**D**
val	arg	leu	asp	phe	asp	val	tyr	asn	his	tyr	tyr
E	**F**	**101**	**102**	103	104	105	106	107	108	109	110
val	leu	asp	tyr	trp	gly	gln	gly	thr	ser	val	thr
111	112	113									
val	ser	ser									

the superimposition of the HC19 V_L and J539 V_H domains, residues H90 to H104 (the CDR H3-containing loop) of the J539 V_H domain were replaced by the corresponding loop residues from HC19 to form a HC19 V_L-J539 V_H chimera with the H3 loop from HC19. All residues were then manually modified, or mutated, to reflect the 34E4 sequence. For the "mutated" residues, the side-chain rotamer that gave the best fit to the local environment as judged by visual inspection was chosen. Other known structures were also consulted in remodeling the local sequence environment around the mutated residues when the change required a significant structural alteration. For example, replacing Met^{H82} with a branched leucine in the J539 V_H domain caused a steric clash with the surrounding residues. However, structural information from antibody CHA255 (1ind.pdb),[46] which has a leucine residue at position H82, helped resolve the problem.

Quantum Mechanical Methods. Both transition state geometries were optimized in the gas phase with Density Functional Theory (DFT)[47] at B3LYP/6-31+G(d) level with GAUSSIAN 98.[18] CHELPG[48] charges were obtained at B3LYP/6-31+G(d) level. Several solvation models including CPCM,[19] a polarizable conductor-like solvation model, PCM,[20] a polarizable continuum model, a Poisson−Boltzmann (PB) model[21] and the Cramer−Truhlar SM5.2R solvation model[22] were compared for solvation calculations on acetate-catalyzed reaction (Table 4). All solvation energies from continuum models (PCM and CPCM) are single point energies computed based on the geometries in the gas phase.

Table 4. Comparison of Experimental and Calculated Solvation Free Energies and Nitrobenzisoxazole Elimination Activation Energies for Acetate-Catalysis with Different Theoretical Models

	solvation free energy in H_2O (kcal/mol)				solvation free energy in CH_3CN (kcal/mol)			
	AcO^-	NBI	TS	$\Delta\Delta G^‡$	AcO^-	NBI	TS	$\Delta\Delta G^‡$
CPCM[a]	−74.1	−5.2	−43.0	28.6	−63.0	−0.6	−33.6	22.2
PCM[a]	−75.3	−6.7	−43.5	30.7	−63.4	−0.6	−33.6	22.6
PB[b]	−77.4	−5.7	−46.4	28.9	−75.1	−12.4	−54.4	25.3
SM5.2R[c]	−77.3	−11.4	−51.6	29.3	−75.6	−15.7	−56.3	27.2
experiment	−77.0[d]			23.8	−62.7[e]			13.1

[a] B3LYP/6-31+G* with CPCM or PCM solvation models in Gaussian 98. [b] B3LYP/6-31+G* with Poisson−Boltzmann solvation model in Jaguar 4.0.[21] [c] AM1 with SM5.2R solvation model in AMSOL 6.5.[22] [d] Ref 23. [e] Pliego, Jr., J. R.; Riveros, J. M. *Phys. Chem. Chem. Phys.* **2002**, *4*, 1622.

Docking Calculations. Autodock 3.0[26] was employed for docking purposes. Autodock uses a hybrid Lamarckian genetic algorithm (LGA) for docking and predicts the best binding modes according to an empirical scoring function that predicts the binding energy. Acetate was left out purposely from the gas-phase transition state docking experiments, since a carboxylate of an aspartate or glutamate in the binding site is considered to be the base. CHELPG charges were taken from the computed transition state structure in the gas phase. The receptor is fixed in all the dockings and represented by grid maps. The transition states do not have any torsional degrees of freedoms because of their structural rigidity. A total of 100 ga-run were conducted in each case and resulting conformations were clustered with 1 Å root-mean-square deviations (RMSD). The representative docked conformation of the best cluster in terms of binding free energy and population was chosen as the final binding mode.

Location of Binding Sites in HSA. The CASTp program was used to locate possible binding cavities and pockets for albumin using a solvent probe (sphere of 1.4 Å) analytically.[28] Multiple binding pockets and cavities for HSA (PDB ID: 1BJ5) have been found as shown in Figure 8 (top). This crystal structure includes five bound myristic acids. These were removed for the CASTp analysis. The spheres represent the surfaces of the key C, N, and O atoms that define the boundary between bulk solvent and protein pockets or cavities.

Acknowledgment. We thank Jim Na (Pfizer, La Jolla), Jeehiun K. Lee (Rutgers), and Qiaolin Deng (Merck) for preliminary results and extensive discussions. We are grateful to the National Institute of General Medical Sciences, National Institutes of Health (D.H. and K.N.H.) and National Science Foundation (K.N.H.) for financial support of this research and to the Naito Foundation (Tokyo, Japan) for a postdoctoral fellowship to K.K. We owe special thanks to UCLA Academic Technology Services (Y.H. and K.N.H.) and ETH and Novartis (D.H.).

JA0490727

(46) Love, R. A.; Villafranca, J. E.; Aust, R. M.; Nakamura, K. K.; Jue, R. A.; Major, Jr., J. G.; Radhakrishnan, R.; Butler, W. F. *Biochemistry* **1993**, *32*, 10 950−10 959.

(47) (a) Becke, A. D. *J. Chem. Phys.* **1993**, *98*, 5648−5652. (b) Lee, C. T.; Yang, W. T.; Parr, R. G. *Phys. Rev. B* **1988**, *37*, 785−789.

(48) (a) Chirlian, L. E.; Francl, M. M. *J. Comput. Chem.* **1987**, *8*, 894−905. (b) Breneman, C. M.; Wiberg, K. B. *J. Comput. Chem.* **1990**, *11*, 361−373.